Exploring the Structure of Galaxy Clusters: XMM-Newton observations of the REFLEX-DXL clusters at $z \sim 0.3$ ⋆

Y.-Y. Zhang [a], H. Böhringer [a], A. Finoguenov [a], Y. Ikebe [a,b], K. Matsushita [a,c], P. Schuecker [a], L. Guzzo [d], C. A. Collins [e]

[a] *Max-Planck-Institut für extraterrestrische Physik, Garching, Germany*

[b] *Joint Center for Astrophysics, University of Maryland, Baltimore, USA*

[c] *Tokyo University of Science, Tokyo, Japan*

[d] *INAF-Osservatorio Astronomico di Brera, Merate/Milano, Italy*

[e] *Liverpool John Moores University, Liverpool, U.K.*

Abstract

The precise determination of global properties of galaxy clusters, and their scaling relations, is a task of prime importance for the use of clusters as cosmological probes. We performed a detailed XMM-Newton study of 14 X-ray luminous REFLEX Survey clusters at $z \sim 0.3$. We found that the properties of the galaxy clusters show a self-similar behavior at $r > 0.1 r_{\rm vir}$. This helps to establish tighter scaling relations. Peculiarities in the individual clusters are important to understand the scatter from the self-similar frame in the cluster central parts.

Key words: Large scale structure of the Universe, Galaxy clusters, Observational cosmology

1 Introduction

ROSAT and ASCA observations (e.g. Markevitch et al. 1998; Vikhlinin et al. 1999; Arnaud et al. 2002; Reiprich and Böhringer 2002) and simulations

⋆ This work is based on observations made with the XMM-Newton, an ESA science mission with instruments and contributions directly funded by ESA member states and the USA (NASA).

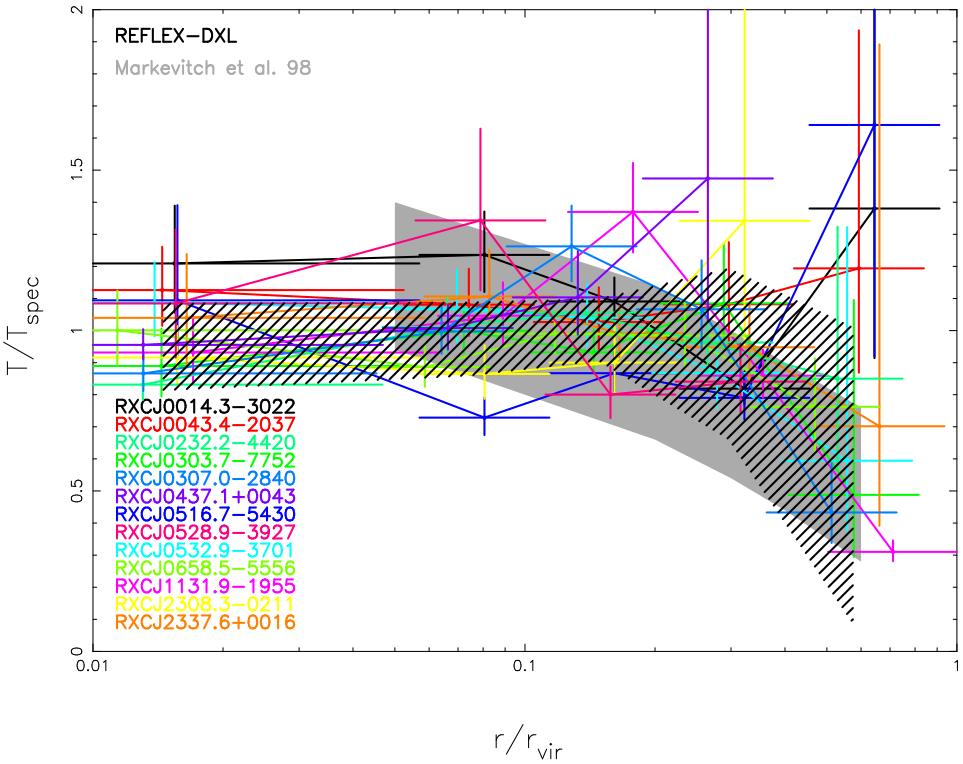

Fig. 1. Scaled temperature profiles. The shadow shows a weighted temperature profile of the REFLEX-DXL clusters (hatched) and the temperature profile range in Markevitch et al. (1998; filled).

(e.g. Kay 2004; Borgani 2004) indicate a self-similar form of the intracluster medium (ICM) properties such as temperature, density, and entropy for massive clusters ($k_{\rm B}T > 4$ keV) excluding cooling cores (Fabian and Nulsen 1977). XMM-Newton has the advantage of high spectral resolution and large field of view (FOV) for detailed studies. This helps us to compose an almost volume complete sample of 13 distant, X-ray luminous (DXL; $z = 0.27$ to 0.31; $L_X \geq 10^{45}$ erg s^{-1} for $0.1 - 2.4$ keV) galaxy clusters and one supplementary cluster at $z = 0.2578$ from the ROSAT-ESO Flux-Limited X-ray (REFLEX; Böhringer et al. 2004) galaxy cluster survey. We correct the volume completeness with a known selection function for distant, X-ray luminous clusters ($L_X \geq 10^{45}$ erg s^{-1}) as described in Böhringer et al. (2005; Paper I). A prime goal for the study of the REFLEX-DXL sample is to obtain spatially resolved ICM properties such as the temperature (Zhang et al. 2004a; Paper II), to derive accurate measurements of the cluster mass and gas mass fraction, and to study the peculiarities in the cluster structure which introduce a scatter in the scaling relations. We adopt a flat ΛCDM cosmology with $\Omega_{\rm m} = 0.3$ and $H_0 = 70$ km s^{-1} Mpc^{-1}. Confidence intervals correspond to the 68% confidence level.

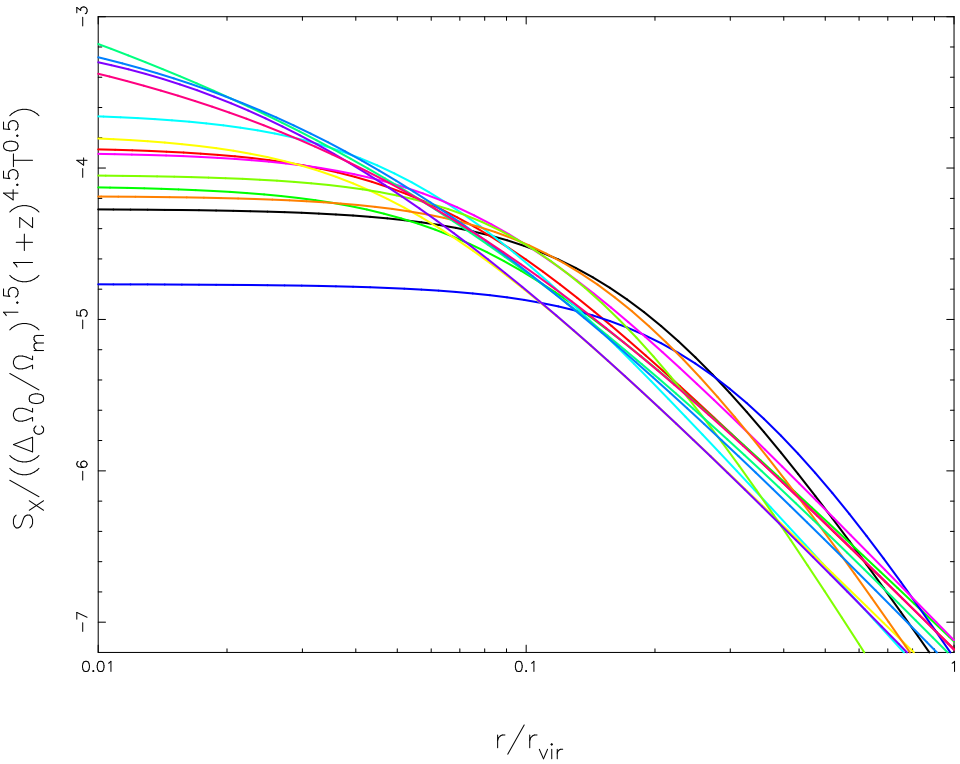

Fig. 2. The best surface brightness model fits (PSF deconvolved) scaled to the self-similar frame for pn. The color coding is the same as used for Fig. 1. The typical uncertainty of the surface brightness increases from 10% to 20% from the inner parts to the outer parts.

2 Data reduction

We use the XMMSAS v6.0 software for data reduction. For pn data, the fractions of the out-of-time (OOT) effect are 2.32% and 6.30% for Extend Full Frame (EFF) and Full Frame (FF) mode, respectively. We create an OOT event list file and statistically remove the OOT effect. To avoid the episodes of "soft proton flares" (De Luca & Molendi 2004), we use a threshold of 3σ clipping to clean the data in both the hard band (10–12 keV band and 12–14 keV band for MOS and pn, respectively) and the soft band (0.3–10 keV band).

Over half of the clusters clearly show substructures or/and elongation. We use "edetect_chain" to detect point-like sources. We subtract the substructures and point-like sources leaving only the main component.

The observations of RXCJ2011.3−5725 are contaminated by flares. Thus we only obtain a global temperature ($\sim$ 3.77 keV). Some properties of these observations and an overview of the sample are described in Paper I. We obtained the temperature profiles of 9 REFLEX-DXL clusters in Paper II. Also included in this paper are the observational parameters, alternative names, data prepa-

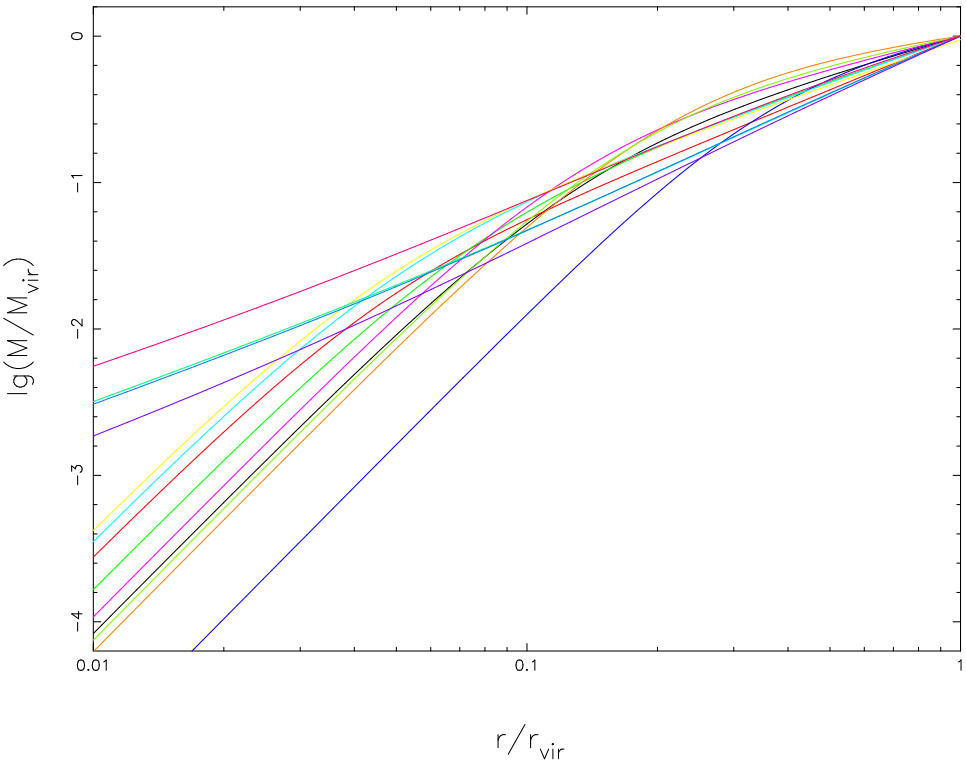

Fig. 3. Scaled X-ray mass profiles of the REFLEX-DXL clusters. The color coding is the same as used for Fig. 1. The typical uncertainty of the mass increases from 10–40% to 25–80% from the inner parts to the outer parts.

ration and double background subtraction method which is developed to provide a precise spectral background removal. We apply the XMM-Newton blank sky pointings in the Chandra Deep Field South (CDFS) as background.

3 ICM properties

We have considered the projection effects over the line of sight in the temperature and surface brightness measurements. We have accounted for the PSF effect for surface brightness. In the spectral analysis, we have applied a large radial binning, greater than $0.5'$, to reduce the PSF effect instead of accounted for the PSF blurring completely because of limited photon statistics. This should be considered for the reliability of the temperature profiles in the central part. For such distant clusters, the PSF effect is important within $0.3r_{\rm vir}$ which introduces an added uncertainty to the final results. This can only be investigated using deep exposures with better photon statistics.

3.1 Temperature distribution

We perform the spectral analysis in five annuli: 0–0.5′, 0.5–1′, 1–2′, 2–4′, and 4–8′, to measure the temperature profiles. We applied both the residual spectrum (e.g. Arnaud et al. 2002; Zhang et al. 2005) and a "powerlaw" model (Zhang et al. 2004a) to account for the residual background in the double background subtraction method (Zhang et al. 2004a) for spectral background removal. We found that the two methods provide consistent results within 1 σ error except for the last annulus for RXCJ0232.2−4420 and RXCJ1131.9−1955. The disagreement is caused by the underestimate/overestimate of the formal errors in the measurements using a residual model/spectrum. We deprojected the temperature profiles and found consistent results within 1 σ error bars.

We apply the global spectral temperatures and $r_{\rm vir}$ to scale the temperature profiles (see Fig. 1). Excluding the individual data points with error bars over 150% of the mean value, we derived a weighted temperature profile of the REFLEX-DXL clusters. We found a closely self-similar behavior with a constant distribution at $r < 0.3r_{\rm vir}$ and a decrease at $r > 0.3r_{\rm vir}$. This averaged temperature profile keeps an overall agreement with the one in Markevitch et al. (1998). A similar universal temperature profile is indicated in simulations (Borgani et al. 2004; Borgani 2004).

3.2 Surface brightness

We choose the 0.5–2 keV band to derive surface brightness profiles (also see Zhang et al. 2005). This provides an almost temperature-independent X-ray emission coefficient over the expected temperature range. We derive the azimuthally averaged surface brightness of the XMM-Newton blank sky pointings in the same detector coordinates as for the targets. The count rate ratio of the targets and CDFS in the 10–12 keV band and 12–14 keV band for MOS and pn, respectively is used to scale the CDFS surface brightness. The data are rebinned to ensure (1) at leat 100 counts (30 counts for a limited photon statistics case) per bin, and (2) 3-σ source count rate. We subtract the scaled CDFS surface brightness and obtain the surface brightness including the cluster surface brightness and a residual soft X-ray background. This residual background is flat over the FOV. It is estimated in the outer region ($11' < r < 15'$). We fit the cluster surface brightness profile by a surface brightness prediction convolved with the XMM-Newton Point Spread Function (PSF; Ghizzardi 2001).

Four (RXCJ0232.2−4420, RXCJ0307.0−2840, RXCJ0437.1+0043 and RXCJ0528.9−3927) of 13 clusters show pronounced or moderate cooling flows. For the remaining 9

clusters, a β-model provides a satisfying χ^2 fit of the surface brightness profiles in the observed radial range. The surface brightness profiles (see Fig. 2) are scaled according to the standard self-similar model (e.g. Arnaud et al. 2002) and show a good self-similarity in the $r > 0.1r_{\rm vir}$ region.

3.3 Mass distribution

Surface brightness profiles can be deprojected to yield the emission per volume element, $\xi(r) = \widetilde{\Lambda}(r)n_{\rm e}^2(r)$. This is used to derive ICM density distributions.

For Non-Cooling flow Clusters (NCCs), we make use of the temperature profile and density profile to derive the mass, assuming spherical symmetry and hydrostatic equilibrium. The XMM-Newton mass measurements of the NCCs are consistent with the masses derived from the global temperatures using the observational M_{200}–T relation based on the conventional β model for the X-ray surface brightness profile and hydrostatic equilibrium for 22 nearby clusters from Xu et al. (2001).

Cooling flow Clusters (CCs) show a surface brightness excess in the center. Navarro et al. (1997; $\alpha = 1$; NFW) describe a universal density profile for dark halos from numerical simulations in hierarchical clustering scenarios. This fits the steep X-ray mass profile of CCs in the central region to some degree. An extended-NFW model from recent simulations (e.g. Diemand et al. 2004; Navarro et al. 2004; $\alpha > 1$; ext-NFW) provides an improved fit for such a cuspy profile in the cluster center. For CCs, we make use of the deprojected temperature profile and density profile to parameterize the ext-NFW model under the assumptions of hydrostatic equilibrium, polytropic gas and spherical symmetry. Then the mass is derived from the ext-NFW model.

The typical uncertainty of the mass increases from 10–40% to 25–80% from the inner parts to the outer parts. The NCCs/CCs show shallow/steep mass profiles at the inner parts (Fig. 3). We extrapolate the mass distributions beyond the observed radial range up to the virial radii and scale the mass profiles using the virial mass. The scaled mass profiles (Fig. 3) show a self-similar behavior in the $r > 0.1r_{\rm vir}$ region. The mass concentrations are different for NCCs and CCs in the center.

3.4 Gas mass fraction distribution

The gas mass fraction (see Fig. 4) as a function of radius is derived by $f_{\rm gas}(r) = M_{\rm gas}(r)/M(r)$. At r_{2500}, the gas mass fractions derived from the XMM-Newton exposure of around 10 ks agree with the measurements of

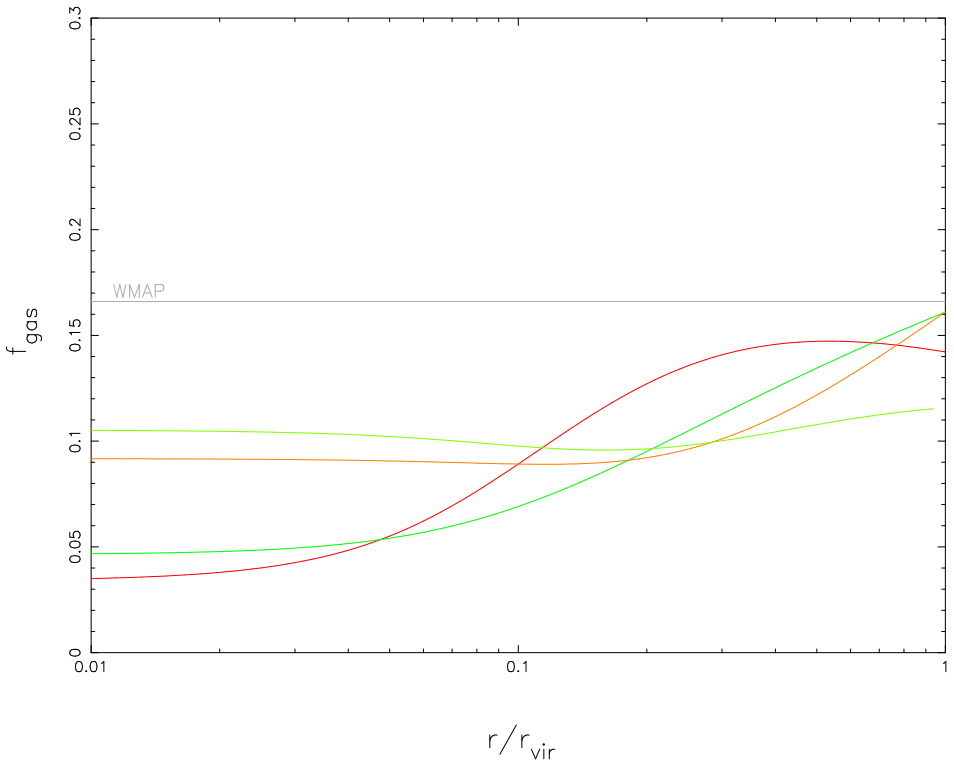

Fig. 4. Gas mass fraction profiles for four typical examples. The WMAP measured baryon fraction of the Universe is $f_{\rm b} = 0.166$, where $\Omega_{\rm b}\ h^2 = 0.0224$ and $\Omega_{\rm m}\ h^2 = 0.135$ (Spergel et al. 2003, horizontal line). The color coding is the same as used for Fig. 1. The typical uncertainty is in the range of 20–70% at $r_{\rm vir}$.

Allen et al. (2004) based on the Chandra observations of 7 clusters yielding $f_{\rm gas} \sim 0.105$–$0.138 h_{70}^{-3/2}$ with similar confidence intervals ($\sim 0.02 h_{70}^{-3/2}$). The gas mass fraction distributions between r_{500} and r_{200} are in the range of $0.12 \sim 0.24$. This is in good agreement with the WMAP measurement of 0.166 (Spergel et al. 2003), the measurements of Ettori et al. (2002) which are based on BeppoSAX observations of 22 nearby clusters, and the measurements of Sanderson et al. (2003) which are based on ASCA/GIS, ASCA/SIS and ROSAT/PSPC observations of 66 clusters yielding $f_{\rm gas} = 0.13 \pm 0.01\ h_{70}^{-3/2}$ at r_{200}. RXCJ0014.3−3022, RXCJ0516.7−5430 and RXCJ1131.9−1955 are in the stage of merger. We obtain slightly higher gas mass fractions in the outskirts artificially caused by the assumption of spherical symmetry.

4 Summary and Discussion

We derive the spatially resolved temperature profiles. We combine the temperature profile with the gas density profile observed up to almost r_{500} to compute accurately the mass and gas mass fraction. An ext-NFW model (β-model) provides a good fit for the CCs (NCCs). X-ray luminous (massive)

galaxy clusters such as the clusters in this paper show a self-similar behavior of their properties, e.g. temperature, density and mass in the $r > 0.1r_{\rm vir}$ region in which we have a good understanding of dark matter.

Peculiarities in the cluster structure introduce a scatter from the self-similar frame in the cluster cores which is due to physical processes rather than simply being statistical fluctuations in the measurement (Zhang et al. 2004b). For example, mergers can not only lead to a temporary increase in the cluster temperature and X-ray luminosity (Randall et al. 2002), but also reduce the surface brightness slope and increase the core radius particular in ongoing cluster mergers (Markevitch et al. 2002), e.g. RXCJ0658.5−5556 and RXCJ0516.7−5430 in our sample. Many studies (e.g. Markevitch et al. 2002; Randall et al. 2002) indicate that the X-ray mass estimate in the center could be biased by the phenomena such as ghost cavities and bubbles that may somehow invalidate the hydrostatic equilibrium hypothesis. More details of the REFLEX-DXL cluster properties, scaling relations, correlations and their scatters will be described in forthcoming papers.

Acknowledgments

YYZ acknowledges receiving the International Max-Planck Research School Fellowship. YYZ would like to thank Hermann Brunner, Michael Freyberg, and Rasmus Voss for providing useful suggestions.

References

Allen, S. W., Schmidt, R. W., Ebeling, H. et al. Constraints on dark energy from Chandra observations of the largest relaxed galaxy clusters. MNRAS 353, 457-467, 2004.

Arnaud, M., Aghanim, N., Neumann, M. The X-ray surface brightness profiles of hot galaxy clusters up to vec $z \sim 0.8$: Evidence for self-similarity and constraints on Ω_0. A&A 389, 1-18, 2002.

Borgani, S. Galaxy clusters as cosmological tools and astrophysical laboratories. Proc. The Riddle of Cooling Flows in Galaxies and Clusters of Galaxies: E4., ed. T. H. Reiprich, J. C. Kempner, & N. Soker, http://www.astro.virginia.edu/coolflow/proc.php?regID=115, 2004.

Borgani, S., Murante, G., Springel, V. et al. X-ray properties of galaxy clusters and groups from a cosmological hydrodynamical simulation. MNRAS 348, 1078-1096, 2004.

Böhringer, H., Schuecker, P., Guzzo, L. et al. The ROSAT-ESO flux limited

X-ray (REFLEX) galaxy cluster survey. V. The cluster catalogue. A&A 425, 367-383, 2004.

Böhringer, H., Schuecker, P., Zhang, Y.-Y. et al. The distant, X-ray luminous galaxy cluster sample from the REFLEX survey (REFLEX-DXL) and its temperature function. A&A submitted, 2005.

De Luca, A., & Molendi, S. The 2-8 keV cosmic X-ray background spectrum as observed with XMM-Newton. A&A 419, 837-848, 2004.

Diemand, J., Moore, B., & Stadel, J. Convergence and scatter of cluster density profiles. MNRAS 353, 624-632, 2004.

Ettori, S., De Grandi, S., Molendi, S. Gravitating mass profiles of nearby galaxy clusters and relations with X-ray gas temperature, luminosity and mass. A&A 391, 841-855, 2002.

Fabian, A. C., Nulsen, P. E. J. Subsonic accretion of cooling gas in clusters of galaxies. MNRAS 180, 479-484, 1977.

Ghizzardi, S. In-flight calibration of the PSF for the MOS1 and MOS2 cameras. EPIC-MCT-TN-011 (Internal report), 2001.

Kay, S. T. The entropy distribution in clusters: Evidence of feedback? MNRAS 347, L13-L17, 2004.

Markevitch, M., Forman, W., Sarazin, C. L. et al. The temperature structure of 30 nearby clusters observed with ASCA: Similarity of temperature profiles. ApJ 503, 77-96, 1998.

Markevitch, M., Gonzalez, A. H., David, L. et al. A Textbook Example of a Bow Shock in the Merging Galaxy Cluster 1E 0657−56. ApJ 567, L27-L31, 2002.

Moore, B., Quinn, T., Governato, F. et al. Cold collapse and the core catastrophe. MNRAS 310, 1147-1152, 1999.

Navarro, J. F., Frenk, C. S., White, S. D. M. A universal density profile from hierarchical clusterin. ApJ 490, 493-508 (NFW), 1997.

Navarro, J. F., Hayashi, E., Power, C. et al. The inner structure of LambdaCDM haloes - III. Universality and asymptotic slopes. MNRAS 349, 1039-1051 (ext-NFW), 2004.

Randall, S. W., Sarazin, C. L., Ricker, P. M. The Effects of Mergers Boosts on the luminosity, temperature and inferred mass functions of clusters of galaxies. ApJ 577, 579-594, 2002.

Reiprich, T. H. & Böhringer, H. The mass function of an X-ray flux-limited sample of galaxy clusters. ApJ 567, 716-740, 2002.

Sanderson, A. J. R., Ponman, T. J., Finoguenov, A. et al. The Birmingham-CfA cluster scaling project - I. Gas fraction and the M–T_X relation. MNRAS 340, 989-1010, 2003.

Spergel, D. N., Verde, L., Peiris, H. V. et al. First-year Wilkinson Microwave Anisotropy Probe (WMAP) observations: Determination of cosmological parameter. ApJS 148, 175-194, 2003.

Vikhlinin, A., Forman, W., Jones, C. Outer regions of the cluster gaseous atmospheres. ApJ 525, 47-57, 1999.

Xu, H.-G., Jin, G.-X., Wu, X.-P. The mass-temperature relation of 22 nearby

clusters. ApJ 553, 78-83, 2001.

Zhang, Y.-Y., Finoguenov, A., Böhringer, H. et al. Temperature gradients in XMM-Newton observed REFLEX-DXL galaxy clusters at $z \sim 0.3$. A&A 413, 49-63, 2004a.

Zhang, Y.-Y., Finoguenov, A., Böhringer, H. et al. Spatial distributions of the REFLEX-DXL galaxy clusters at $z \sim 0.3$ observed by XMM-Newton. Proc. Memorie della Societb Astronomica Italiana - Supplementi in press, astro-ph/0402533, 2004b.

Zhang, Y.-Y., Böhringer, H., Mellier, Y. et al. XMM-Newton study of the lensing cluster of galaxies CL0024+17. A&A 429, 85-99, 2005.